International Journal of Recent Innovations in Academic Research

E-ISSN: 2635-3040; P-ISSN: 2659-1561
Homepage: https://www.ijriar.com/
Volume-10, Issue-3, July-September-2026: 153-162

Research Article

Electrochemical and Surface Characterization of Zinc Corrosion Inhibition by *Ocimum sanctum* Leaf Extract in Hydrochloric Acid

[*a]Kwanchi, I.D., [b]Barminas, J.T., [c]Bassi, K.A. and [b]Rapheal, A.

[a]Department of Industrial Chemistry, Faculty of Physical Sciences, Federal University Wukari, Taraba State, Nigeria
[b]Department of Chemistry, Faculty of Physical Science, Modibbo Adama University, Yola, Nigeria
[c]Department of Chemistry, College of Education Zing, Taraba State, Nigeria
*Corresponding Author Email: kwanchidimas@gmail.com

Article History
Received: August 12, 2026
Accepted: September 02, 2026
Published: September 08, 2026

Abstract

Plant-based corrosion inhibitors are increasingly favoured over synthetic alternatives owing to their low toxicity, biodegradability and cost-effectiveness. However, many studies have emphasized inhibition efficiency while giving less attention to the electrochemical and surface-level evidence of protective film formation. This study evaluated the corrosion protection performance of *Ocimum sanctum* (Holy Basil/Tulsi) leaf extract on zinc in hydrochloric acid (HCl) medium using electrochemical impedance spectroscopy (EIS), scanning electron microscopy (SEM), energy-dispersive X-ray spectroscopy (EDX) and Fourier transform infrared spectroscopy (FTIR). Nyquist plots showed depressed capacitive semicircles whose diameter, and hence charge transfer resistance (Rct), increased from 20 Ω cm^2 for the uninhibited control to 100 Ω cm^2 for zinc coated with 500 mg/dm^3 extract (E500), confirming suppression of the corrosion reaction. Bode modulus and phase angle plots similarly indicated improved barrier and capacitive performance with increasing extract concentration, while equivalent circuit fitting showed an increase in pore resistance (Rpo) from 5.0 to 20.0 Ω cm^2. SEM micrographs revealed a severely pitted and degraded surface for the uninhibited zinc, in contrast to a smooth, compact and largely defect-free surface for E500, consistent with the formation of a protective adsorbed film. EDX analysis showed reduced oxygen enrichment and improved preservation of the zinc signal in inhibited samples, indicating suppressed oxide/corrosion product formation. FTIR spectra of the extract and dried leaf identified hydroxyl, carbonyl, aromatic and amine functional groups associated with phenolics, flavonoids and alkaloids, which are implicated in adsorption onto the zinc surface. The combined electrochemical and surface evidence confirms that *Ocimum sanctum* extract inhibits zinc corrosion in HCl through the formation of a stable, adherent protective film.

Keywords: Zinc Corrosion, *Ocimum sanctum*, Electrochemical Impedance Spectroscopy, SEM/EDX, FTIR, Green Inhibitor.

1. Introduction

Zinc is widely used in galvanization, alloying, and structural applications due to its advantageous mechanical properties and resistance to corrosion (Revie and Uhlig, 2008). However, it is vulnerable to attack in acidic conditions such as hydrochloric acid (HCl), which is commonly utilized in industrial pickling, descaling, and cleaning processes (Pais and Rao, 2021). The health and environmental concerns around synthetic corrosion inhibitors have sparked a growing interest in environmentally friendly alternatives made from plant extracts, which are frequently non-toxic, biodegradable, and reasonably priced (Vashi and Zele, 2020). Flavonoids, tannins, phenolics, and alkaloids are phytochemicals found in the medicinal herb *Ocimum sanctum*, also referred to as holy basil or tulsi, which can chelate metals and form films (Pattanayak *et al.,* 2010; de Souza

Morais *et al.,* 2023). Although weight loss trials have shown the inhibition efficiency of such extracts, direct electrochemical and microscopic evidence of protective layer development is required to verify the underlying inhibitory mechanism (Popova *et al.,* 2003). Electrochemical impedance spectroscopy (EIS) illuminates interfacial charge transfer processes, while scanning electron microscopy (SEM), energy-dispersive X-ray spectroscopy (EDX), and Fourier transform infrared spectroscopy (FTIR) offer complementary morphological, elemental, and functional group evidence of inhibitor adsorption (Silverstein *et al.,* 2014; Goldstein *et al.,* 2018).

In order to provide direct electrochemical and surface-level evidence that complements the gravimetric inhibition results and offers a more comprehensive understanding of the inhibition mechanism, this study examined the corrosion protection behavior of *Ocimum sanctum* leaf extract on zinc in hydrochloric acid solution using EIS, SEM, EDX and FTIR. The electrochemical processes taking place at the metal–solution interface and the physicochemical makeup of the protective layer created by the inhibitor are not sufficiently revealed by weight-loss measurements, even though they offer quantitative data on the overall corrosion rate and inhibition efficiency over a 3-hours exposure period.

Because it allows the assessment of charge transfer resistance, double-layer capacitance, solution resistance, and adsorption characteristics without substantially disrupting the corrosion system, EIS is one of the most sensitive and popular methods for examining corrosion processes. The Nyquist and Bode impedance graphs produced by EIS offer important details on the kinetics of electrochemical reactions taking place at the metal surface. The degree of corrosion damage and the efficacy of the protective layer created by plant-derived inhibitors can be directly observed through surface morphological examination using SEM. Due to aggressive chloride ion attack, corroded zinc surfaces submerged in uncontrolled acidic environments usually show significant pitting, fractures, roughness, localized dissolving, and substantial surface deterioration. Zinc surfaces exposed to inhibited solutions, on the other hand, typically exhibit smoother, more uniform morphologies with noticeably fewer corrosion defects, indicating the creation of a compact adsorbed layer that protects the substrate from acid attack. As a result, SEM observations provide crucial qualitative proof for the protective activity deduced from electrochemical and gravimetric measurements.

EDX was used to measure changes in the elemental composition of the zinc surface after exposure to corrosive media both with and without *Ocimum sanctum* extract in order to supplement the morphological observations. The relative quantity of metallic zinc, oxygen and carbon on the corroded surface can be determined semi-quantitatively using EDX analysis. Following inhibitor treatment, a decrease in oxygen and chlorine signals and an increase in carbon content are typically regarded as proof of organic molecule adsorption and the inhibition of corrosion product formation.

Additionally, the functional groups in the plant extract were characterized both before and after interaction with the zinc surface using Fourier Transform Infrared (FTIR) spectroscopy. Because FTIR analysis detects distinctive vibrational frequencies corresponding to hydroxyl (–OH), amino (–NH), carbonyl (C=O), aromatic (C=C), ether (C–O–C), methoxy ($–OCH_3$), and other heteroatom-containing functional groups with lone-pair electrons capable of coordinating with vacant orbitals of metal atoms, it is especially useful for identifying the phytochemical constituents responsible for adsorption (Silverstein *et al.,* 2014).

2. Materials and Methods

2.1. Zinc Specimen and Extract Preparation

High-purity zinc coupons (6.5 x 3 cm, 0.15 cm thick) were degreased in 95% pure ethanol, cleaned with distilled water, and stored in a desiccator before use ASTM E1508-18, 2018). *Ocimum sanctum* leaves were rinsed, air-dried, and ground before being extracted using Soxhlet extraction in 95% ethanol at 80 °C for six hours. The filtrate was concentrated by rotary evaporation at 40 °C and reconstituted to concentrations of 100–500 mg/dm^3 for the corrosion protection experiments at 500 mg/dm^3 at room temperature.

2.2. Electrochemical Impedance Spectroscopy (EIS)

The EIS results showed a clear improvement in the corrosion resistance of zinc in the presence of *Ocimum sanctum* extract. The Nyquist plots displayed depressed capacitive semicircles, indicating that charge-transfer processes at the zinc/solution interface played an important role in the corrosion reaction. The diameter of the semicircles increased with increasing extract concentration, while the charge-transfer resistance (Rct) increased from 20 Ω cm^2 for the control to 100 Ω cm^2 at 500 mg/dm^3 extract. This increase in Rct suggests that the presence of the plant extract made it more difficult for the electrochemical corrosion reactions to occur at the zinc surface. The increase in pore resistance (Rpo), from 5.0 Ω cm^2 for the control to 20.0 Ω cm^2 for the

sample containing 500 mg/dm^3 extract, further suggests that the protective layer became more effective in limiting the movement of corrosive species through the surface layer (Popova *et al*., 2003). The Bode plots also showed an increase in impedance magnitude with increasing extract concentration, particularly at lower frequencies. This behaviour indicates an improvement in the barrier properties of the zinc surface. Similarly, the changes observed in the phase angle response suggest that the presence of the extract altered the electrochemical behaviour of the metal/solution interface. Taken together, the EIS results suggest that increasing the concentration of *Ocimum sanctum* extract improves the resistance of zinc to corrosion, most likely through the formation of a protective layer on the metal surface.

2.3. Scanning Electron Microscopy (SEM)

Zinc coupons (control, uninhibited at 0.1 and 0.5 M HCl, and inhibited at 100 and 500 mg/dm^3 extract) were degreased, rinsed, dried, and mounted on SEM stubs using conductive carbon tape for high-resolution imaging of surface morphology, pitting, and film formation (Jones, 2013; ASTM E1508-18, 2018).

2.4. Energy-Dispersive X-Ray Spectroscopy (EDX)

To ascertain the elemental composition of the zinc surface both before and after treatment, EDX analysis was carried out in tandem with SEM. In order to provide a sufficient signal-to-noise ratio, specimen was placed on conductive stubs, and spectra were obtained at an accelerating voltage of 15–20 kV, a working distance of roughly 10 mm, and live acquisition periods of 60–100 seconds (Goldstein *et al*., 2018).

2.5. Fourier Transform Infrared Spectroscopy (FTIR)

FTIR analysis was used on dry *Ocimum sanctum* leaf powder, the concentrated extract, and untreated zinc coupons to identify functional groups (such as -OH, -C=O, and -NH_2) associated with metal-inhibitor interactions (Abiola and James, 2010). While dried extract residues were examined using attenuated total reflectance (ATR)-FTIR without pellet preparation, zinc coupons were examined directly by placing the flat surface on the ATR crystal. Spectra were recorded, annotated, and linked in accordance with recognized functional group allocations (Coates, 2000; Silverstein *et al.,* 2014).

3. Results and Discussion

Table 1. FTIR absorption bands of dried powdered *Ocimum sanctum* leaf.

Wavenumber (cm^{-1})	Functional group	Proposed compound
3315–3183	O–H stretching	Phenols, alcohols
3015	Aromatic C–H	Essential oils
2916	Aliphatic C–H	Terpenoids
2849	C–H stretching	Hydrocarbons
1733	C=O stretching	Esters, ketones
1600	C=C stretching	Aromatic rings
1541	N–H bending	Alkaloids
1375–1239	C–N/C–O stretching	Phenolics
1144	C–O stretching	Flavonoids
1008	C–O–C stretching	Glycosides

Table 2. FTIR bands of crude extract.

Wavenumber (cm^{-1})	Functional group	Assignment
3365.79	O–H stretching	Phenolics
3291.24	N–H stretching	Amines
1707.12	C=O stretching	Carbonyl
1686.62	Conjugated carbonyl	Ketones
1617.66	Aromatic C=C	Phenolics
1507.71	Aromatic ring	Eugenol
1272.89	C–O stretching	Phenols
1224.3	C–N stretching	Amines
1171.1	C–O stretching	Alcohols
1033.4	C–O stretching	Glycosides
721.24	C–H bending	Aromatic ring
678.38	C–Cl stretching	Substituted aromatics
661.60	C–H bending	Halogenated compounds

Table 3. FTIR analysis of untreated zinc surface.

Wavenumber (cm^{-1})	Functional group	Assignment
661.60	Zn–O stretching	Zinc oxide (ZnO)
687.69	Zn–OH vibration	Zinc hydroxide ($Zn(OH)_2$)
758.51	CO_3^{2-} out-of-plane bending	Carbonate species
780.88	Zn–O stretching	Zinc oxide (ZnO)
862.88	CO_3^{2-} out-of-plane bending	Zinc carbonate
2851–2956	C–H stretching	Surface hydrocarbon contaminants
3203–3602	O–H stretching	Adsorbed water and surface hydroxyl groups

Table 4. Electrochemical parameters.

Sample	Rs (Ω cm^2)	Rpo (Ω cm^2)	Rct (Ω cm^2)
Control	2.3	5.0	20
100 mg dm^3	2.5	10.5	45
300 mg dm^3	2.4	15.0	70
500 mg dm^3	2.2	20.0	100

Table 5. Elemental composition of zinc surface.

Sample	Zinc (%)	Oxygen (%)	Carbon (%)
Control	52.3	42.5	5.2
100 mg dm^3	68.0	29.4	5.8
300 mg dm^3	72.5	21.2	6.3
500 mg dm^3	81.4	12.7	5.9

3.1. FTIR Analysis of Dried *Ocimum sanctum* Leaf

The dried *Ocimum sanctum* leaf's FTIR spectroscopy (Figure 1) showed multiple absorption bands that were in line with its main phytoconstituents. O-H stretching of phenolic and alcoholic hydroxyl groups was identified as a broad band between 3315 and 3183 cm^{-1} (Silverstein *et al*., 2014), whereas aromatic and aliphatic C-H stretching, which indicated terpenoid and essential oil components, corresponded to peaks at 3015, 2916, and 2849 cm^{-1} (Coates, 2000). C=O stretching of esters, aldehydes, ketones, or carboxylic acids was identified as the cause of a strong band at 1733 cm^{-1}, indicating oxygenated substances such flavonoids and phenolic acids that can form coordinating bonds with the metal surface. While bands in the 1375-1239 cm^{-1} range were attributed to C-N and C-O stretching of amines, phenols, and ethers, bands at 1600 and 1541 cm^{-1} showed aromatic C=C stretching and N-H bending, confirming aromatic and nitrogen-containing (alkaloid) compounds. The C-O and C-O-C stretching characteristic of glycosidic linkages and flavonoid glycosides was represented by peaks at 1144 and 1008 cm^{-1}.

3.2. FTIR Analysis of *Ocimum sanctum* Crude Extract

The ethanolic extract's FTIR spectrum (Figure 2) revealed distinctive absorption bands that were consistent with terpenoids, phenolics, flavonoids, and aromatic chemicals. While the band at 1033.4 cm^{-1} corresponded to C-O stretching of phenolic hydroxyl and glycosidic linkages, consistent with the presence of eugenol and related phenolic derivatives, the bands at 661.60, 678.38, and 721.24 cm^{-1} C-H out-of-plane bending, typical of substituted aromatic rings in phenolics and flavonoids (Prakash and Gupta, 2005). The C-O stretching of phenols and the C-N stretching of amines, which both promote electron donation to the metal surface during adsorption, were identified as the peaks at 1171.1, 1224.3, and 1272.89 cm^{-1}. While bands at 1686.62 and 1707.12 cm^{-1} were attributed to C=O stretching of conjugated carbonyl compounds that might coordinate with the zinc surface, bands at 1507.71 and 1617.66 cm^{-1} corroborated the aromatic C=C stretching characteristic of eugenol-type structures. The presence of phenolic and amine functionalities linked to the extract's antioxidant and corrosion-inhibitory activities was supported by broad bands at 3291.24 and 3365.79 cm^{-1}, which verified O-H and potentially N-H stretching.

3.3. FTIR Analysis of Untreated Zinc Surface

The untreated zinc surface's FTIR spectrum (Figure 3) revealed bands at 661.60, 687.69, 758.51, 780.88, and 862.88 cm^{-1}, which were ascribed to carbonate out-of-plane bending and Zn-O and Zn-OH vibrations, suggesting the spontaneous formation of zinc oxide and hydroxide layers upon exposure to air (Revie and Uhlig, 2008; Nakamoto, 2009). While a wide band between 3203 and 3602 cm^{-1} suggested O-H stretching from adsorbed water and surface hydroxyl groups, compatible with zinc hydroxide production under humid conditions, bands between 2851 and 2956 cm^{-1} were attributed to C-H stretching from surface contaminants.

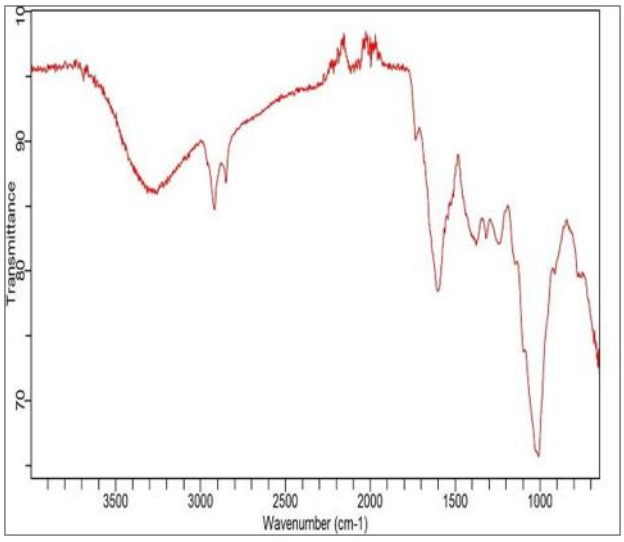

Figure 1. FTIR spectrum of *Ocimum sanctum* powdered leaf.

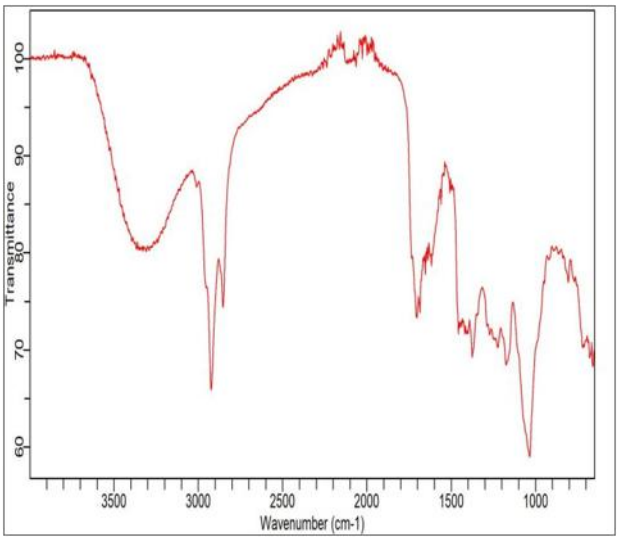

Figure 2. FTIR spectrum of *Ocimum sanctum* crude extract.

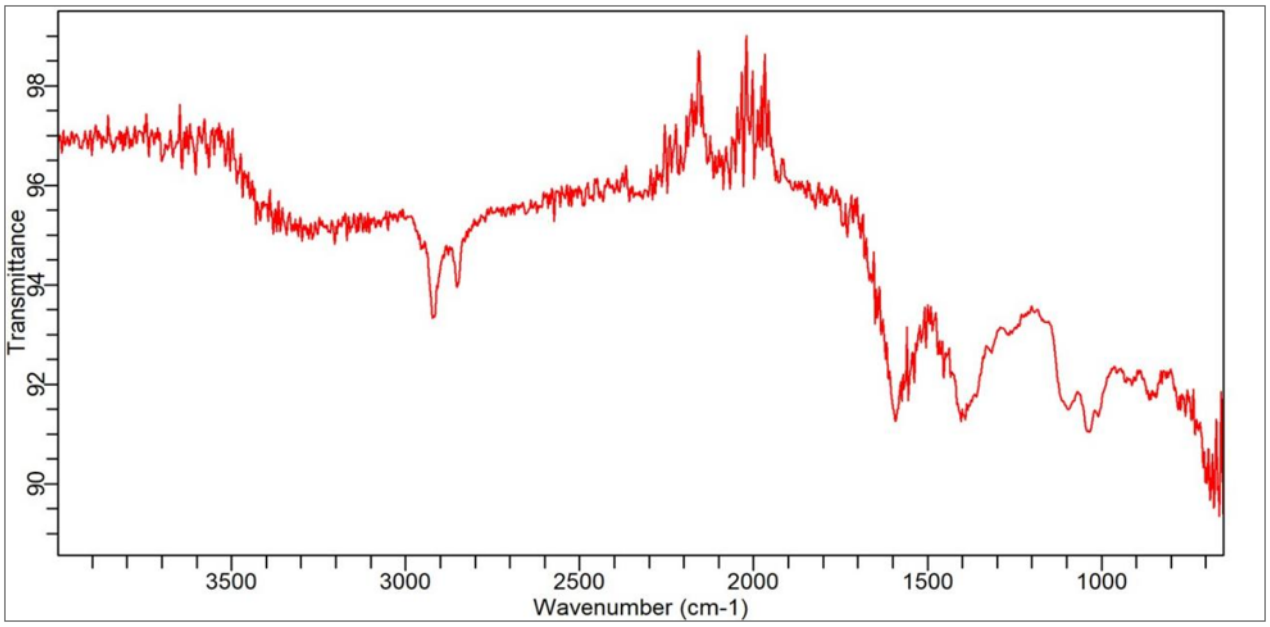

Figure 3. FTIR spectrum of untreated zinc sample.

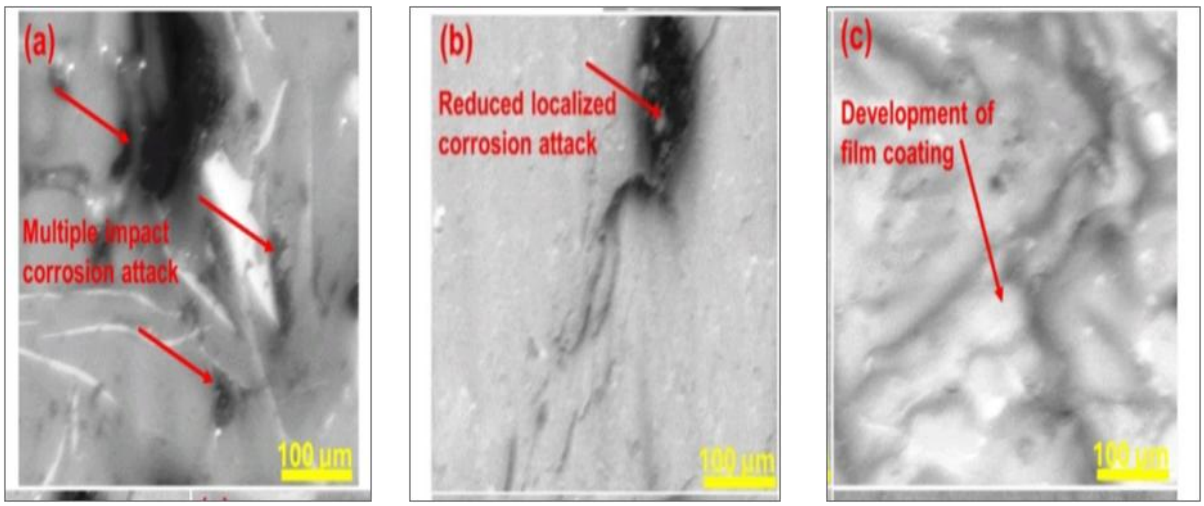

Figure 4a. Control. **Figure 4b.** Uninhibited at 0.1 M. **Figure 4c.** Uninhibited at 0.5 M.

Figure 4. SEM morphology of control and uninhibited zinc coupons.

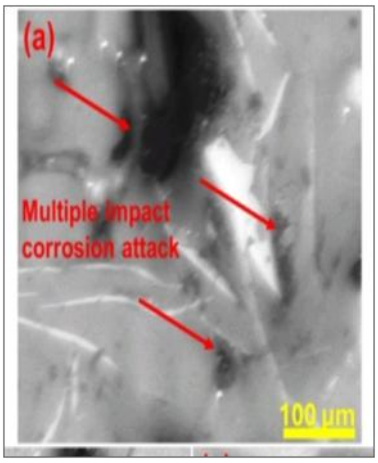

Figure 5a. Control.

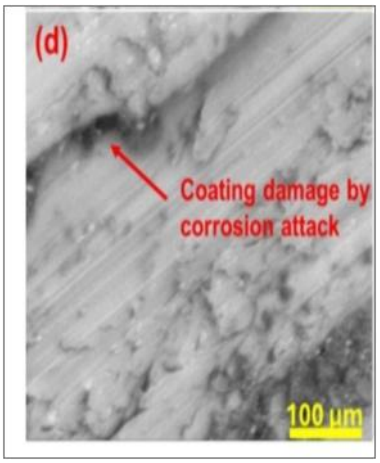

Figure 5d. Inhibited in 100mg/dm^3.

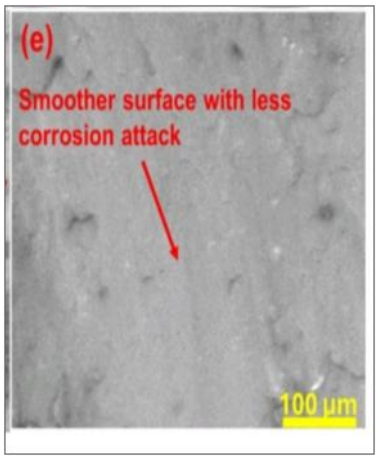

Figure 5e. Inhibited in 500 mg/dm^3.

Figure 5. SEM morphology of control and inhibited zinc coupons.

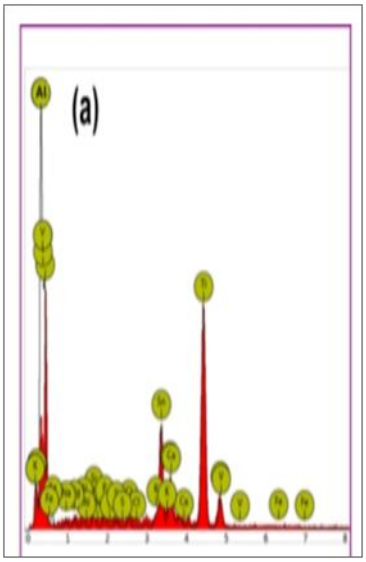

Figure 6a. Control.

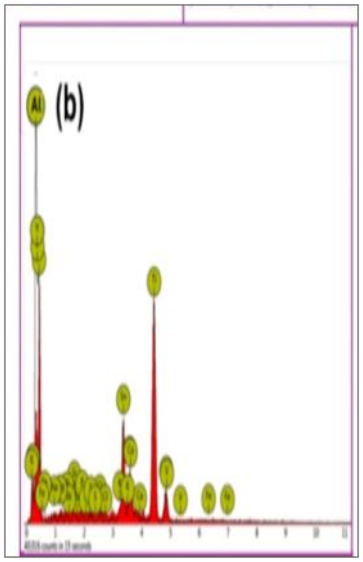

Figure 6b. Uninhibited at 0.1 M.

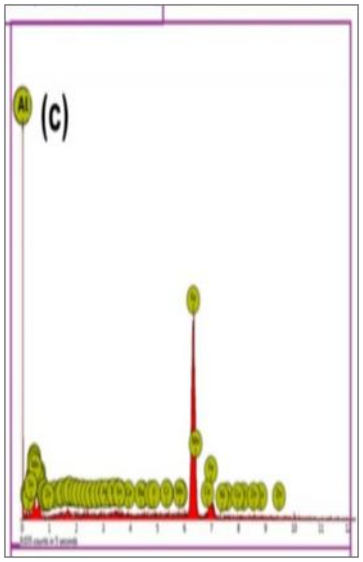

Figure 6c. Uninhibited at 0.5 M.

Figure 6. EDX of control and uninhibited zinc coupons.

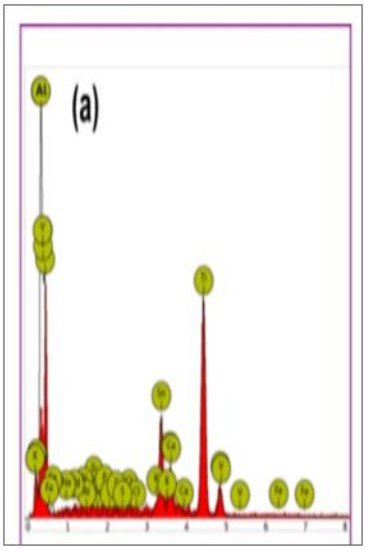

Figure 7a. Control.

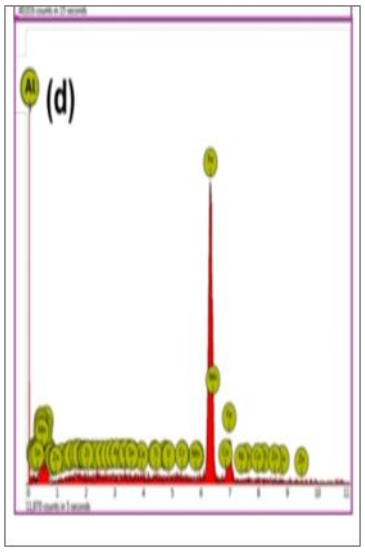

Figure 7d. Inhibited in 100mg/dm^3.

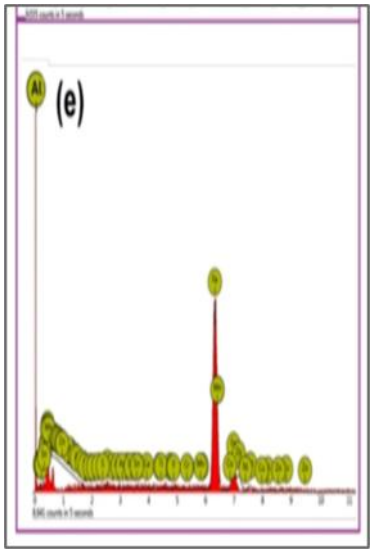

Figure 7e. Inhibited in 500 mg/dm^3.

Figure 7. EDX of control and inhibited zinc coupons.

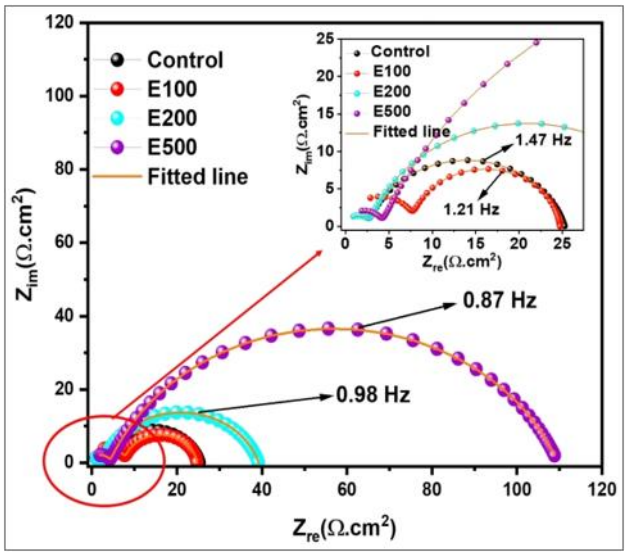

Figure 8. Nyquist plot analysis for EIS.

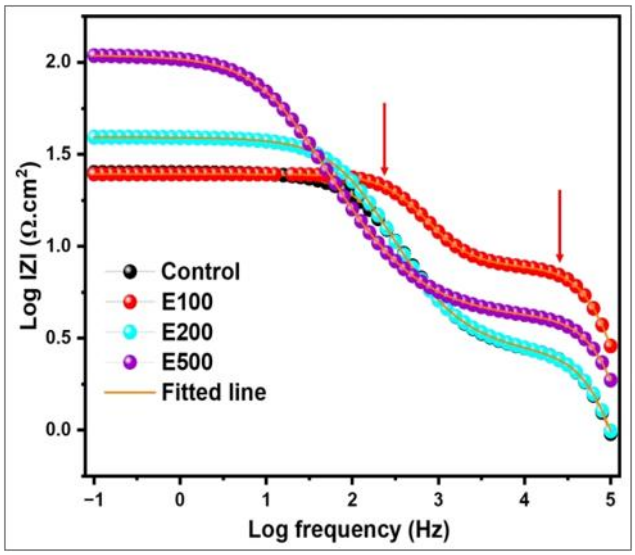

Figure 9. Bode modulus plots for EIS.

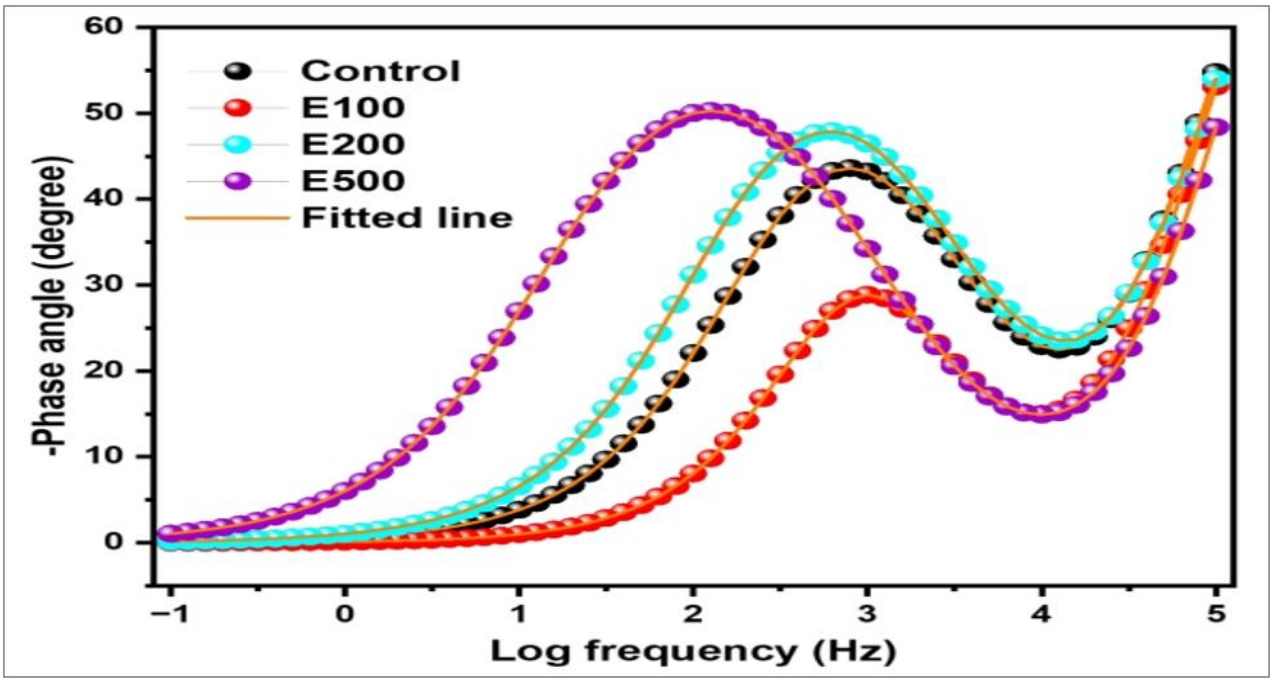

Figure 10. Bode phase angle plots for EIS.

Electrochemical impedance spectroscopy (EIS) analysis of coated Zinc in Figure 8,9 and 10 were performed using 500mg/dm^3 of inhibitor at corrosion environment at room temperature. Where E100 =100mg/dm^3, E200 = 200mg/dm^3 and E 500= 500mg/dm^3.

3.4. Nyquist Plot Analysis

Nyquist plots (Figure 8) for zinc in 500mg/dm^3 showed depressed capacitive semicircles, suggesting that charge transfer at the metal/electrolyte interface dominated the corrosion process. The depression was attributed to surface heterogeneity and frequency dispersion, which are usually modeled using constant phase elements. Charge transfer resistance increased from 20 to 100 Ω cm^2, corresponding to a five-fold improvement in corrosion resistance for E500, indicating a significant suppression of the corrosion reaction. A steady increase in semicircle diameter was seen from the control to E500. According to related research on coated zinc systems in acidic conditions, this rise in Rct is consistent with the development of a compact, adherent protective coating that restricts chloride ion penetration and inhibits electrochemical corrosion reactions.

3.5. Bode Modulus and Phase Angle Analysis

In line with the results of Khan *et al.,* (2022), Bode modulus plots (Figure 9) demonstrated that impedance magnitude increased with increasing extract concentration, especially in the low-frequency region linked to

coating barrier performance. The higher impedance seen for E500 indicated superior corrosion protection. Reduced electrolyte transport through coating pores and flaws was demonstrated by the equivalent rise in pore resistance (Rpo), which went from 5.0 Ω cm^2 for the control to 20.0 Ω cm^2 for E500. As extract concentration increased, Bode phase angle plots also revealed wider and higher phase angle peaks, indicating enhanced dielectric behavior and surface homogeneity and verifying the existence of a stable protective film that postpones interfacial corrosion reactions (Minhas *et al*., 2022; Zhang *et al*., 2024).

3.6. Electrochemical Equivalent Circuit Analysis

An equivalent circuit with solution resistance (Rs), pore resistance (Rpo), charge transfer resistance (Rct), and two constant phase elements (Q1 and Q2), which represent the coating/electrolyte and metal/electrolyte interfaces, respectively, was fitted to the impedance data (Zhang *et al*., 2024). The comparatively little variance in Rs amongst the systems suggested that coating performance, rather than electrolyte characteristics, was the primary cause of variations in corrosion behavior. While the increase in Rct from 20 to 100 Ω cm^2 for E500 showed significant suppression of corrosion kinetics because corrosion rate is inversely proportional to charge transfer resistance, the increase in Rpo from 5.0 to 20.0 Ω cm^2 confirmed improved coating compactness with increasing extract concentration (Minhas *et al*., 2022).

3.7. SEM Analysis

The SEM images in Figure 4 and 5 provided a clear visual indication of the effect of *Ocimum sanctum* extract on the zinc surface. The control specimen showed a rough and severely damaged surface with visible pits and signs of localized corrosion. The specimen exposed to 0.5 M HCl without the inhibitor also showed considerable surface deterioration, confirming the aggressive nature of the acidic medium (Fouda *et al*., 2024). The sample exposed to 0.1 M HCl appeared less damaged, although some surface defects were still visible. In contrast, the zinc specimens treated with the plant extract showed noticeable improvement in surface appearance. The sample containing 100 mg/dm^3 extract exhibited reduced surface damage, while the specimen treated with 500 mg/dm^3 extract had the smoothest and most uniform surface, with considerably fewer visible corrosion defects. The progressive improvement in surface morphology with increasing extract concentration suggests that the plant extract helped to protect the zinc surface from direct attack by the acidic solution (Wang *et al*., 2024). The SEM observations are also consistent with the EIS results, which showed improved resistance to corrosion in the presence of the extract.

3.8. EDX Analysis

The EDX results in Figure 6 and 7 provided information about changes in the elemental composition of the zinc surface after exposure to the acidic medium. The control sample showed a relatively lower zinc content and a higher oxygen content, which may be related to the formation of zinc oxide, zinc hydroxide, and other corrosion products on the surface. However, the inhibited samples showed an increase in the relative zinc content and a decrease in oxygen content as the concentration of the *Ocimum sanctum* extract increased. The sample treated with 500 mg/dm^3 extract showed the highest relative zinc content and the lowest oxygen content among the tested samples. This suggests that the extract helped to reduce the extent of surface deterioration and the formation of corrosion products (El-Haddad and Fouda, 2025). These observations agree with the SEM results, which showed a smoother and less damaged surface in the presence of the inhibitor. The EDX findings therefore provide additional support for the protective effect of *Ocimum sanctum* extract observed from the electrochemical and surface analyses.

3.9. Correlation of SEM/EDX With Electrochemical Performance

The combined SEM and EDX results confirmed a concentration-dependent enhancement in corrosion protection, with the protective performance following the order E500 > A 0.5 M > E100 > A 0.1 M> Control, where A and E denote uninhibited acid and extract-inhibited samples, respectively. This trend is consistent with the EIS findings, in which E500 exhibited the highest charge transfer resistance, pore resistance and overall corrosion protection, confirming that inhibition occurred through the formation of a compact protective layer that functioned both as a physical barrier and as an electrochemical inhibitor.

3.10. Inhibition Mechanism

The results obtained from the EIS, SEM, EDX, and FTIR analyses provide a consistent picture of the protective action of *Ocimum sanctum* extract on zinc in HCl medium. The plant extract contains several organic compounds with functional groups such as hydroxyl, carbonyl, aromatic, and nitrogen-containing groups. These groups contain atoms with available electron pairs and may interact with the zinc surface, encouraging the adsorption of the extract constituents. As the concentration of the extract increases, more of these organic molecules may become available to cover the exposed areas of the zinc surface. The adsorbed molecules can

act as a protective barrier, reducing the direct contact between the zinc surface and the aggressive species present in the acidic solution. This proposed protective action is reflected in the increased charge-transfer and pore resistance observed from the EIS measurements, the improved surface appearance observed by SEM, and the reduced oxygen content observed in the EDX analysis.

4. Conclusion

The present study shows that *Ocimum sanctum* leaf extract has a promising protective effect against the corrosion of zinc in hydrochloric acid medium. The EIS results showed that the corrosion resistance of zinc improved with increasing extract concentration, as indicated by the increase in charge-transfer resistance and pore resistance. The SEM images also showed a clear improvement in the condition of the zinc surface, with the specimen treated with 500 mg/dm^3 extract showing considerably fewer corrosion defects than the uninhibited samples.

The EDX results further indicated better preservation of the zinc surface and a reduction in oxygen enrichment associated with corrosion-product formation in the presence of the extract. FTIR analysis revealed the presence of hydroxyl, carbonyl, aromatic, and nitrogen-containing functional groups in the plant extract. These functional groups may contribute to the interaction and adsorption of the extract constituents on the zinc surface. In general, the combined results from the electrochemical and surface characterization techniques suggest that *Ocimum sanctum* extract protects zinc by forming an adsorbed protective layer that reduces the interaction between the metal surface and the aggressive acidic environment.

The effectiveness of the extract increased with concentration, with the highest protection observed at 500 mg/dm^3. These findings demonstrate the potential of *Ocimum sanctum* as an environmentally friendly alternative for corrosion protection of zinc in acidic environments. Further studies involving detailed surface chemical analysis, adsorption studies, and long-term exposure tests would be useful to gain a deeper understanding of the protective film and to evaluate the practical application of the extract.

Declarations

Acknowledgments: The authors would like to acknowledge Prof. Barminas, J.T., of the Department of Chemistry, Modibbo Adama University, Yola, for his guidance and support throughout the research work.

Artificial Intelligence (AI) Use Statement: The authors declare that no artificial intelligence (AI)-assisted technologies were used in the conception, design, execution, analysis, interpretation, or writing of this manuscript.

Author Contributions: All authors contributed to the conception and design of the study, experimental work, data analysis and interpretation, and preparation and revision of the manuscript. All authors read and approved the final manuscript.

Conflict of Interest: The authors declare no conflict of interest.

Consent to Publish: The authors consent to the publication of this manuscript in International Journal of Recent Innovations in Academic Research.

Data Availability Statement: The data supporting the findings of this study are available from the corresponding author upon reasonable request.

Funding: This research was funded by the Tertiary Education Trust Fund (TETFund) of Nigeria through an Institutional Based Grant.

Institutional Review Board Statement: Not applicable.

Informed Consent Statement: Not applicable.

Research Content: The research content of this manuscript is original and has not been published elsewhere.

References

1. Abiola, O.K. and James, A.O. 2010. The effects of *Aloe vera* extract on corrosion and kinetics of corrosion process of zinc in HCl solution. Corrosion Science, 52(2): 661–664.
2. ASTM International. 2018. ASTM E1508-18: Standard guide for quantitative analysis by energy-dispersive spectroscopy. ASTM International.
3. Coates, J. 2000. Interpretation of infrared spectra: A practical approach. In: Meyers, R.A., (Ed.), Encyclopedia of analytical chemistry. John Wiley and Sons.
4. de Souza Morais, W.R., da Silva, J.S., Queiroz, N.M.P., de Paiva e Silva Zanta, C.L., Ribeiro, A.S. and Tonholo, J. 2023. Green corrosion inhibitors based on plant extracts for metals and alloys in corrosive environment: A technological and scientific prospection. Applied Sciences, 13(13): 7482.

5. El-Haddad, M.N. and Fouda, A.S. 2025. Investigating *Xanthium spinosum* extract as an eco-friendly corrosion inhibitor for aluminium in acidic environments: A green approach to metal protection. Results in Chemistry, 14: 102136.
6. Fouda, A.E.A.S., Etaiw, S.E.H., Abd El-Aziz, D.M., El-Hossiany, A.A. and Elbaz, U.A. 2024. Experimental and theoretical studies of the efficiency of metal–organic frameworks (MOFs) in preventing aluminum corrosion in hydrochloric acid solution. BMC Chemistry, 18(1): 21.
7. Goldstein, J.I., Newbury, D.E., Joy, D.C., Lyman, C.E., Echlin, P., Lifshin, E., Sawyer, L. and Michael, J.R. 2018. Scanning electron microscopy and X-ray microanalysis (4th ed.). Springer. https://doi.org/10.1007/978-1-4939-6676-9
8. Jones, D.A. 2013. Principles and prevention of corrosion (2nd ed.). Pearson Education.
9. Khan, A.R., Zhang, H.J., Jun, Z., Eldin, S.M., Alsaiari, N.S. and Katubi, K.M. 2022. Electrochemical corrosion resistance of aluminum alloy 6101 with cerium-based coatings in an alkaline environment. Frontiers in Chemistry, 10: 1066958.
10. Minhas, B., Dino, S., Huang, L. and Wu, D. 2022. Active corrosion protection by epoxy coating on Li_2CO_3-pretreated anodized aluminum alloy 2024-T3. Frontiers in Materials, 8: 804328.
11. Nakamoto, K. 2009. Infrared and Raman spectra of inorganic and coordination compounds (6th ed.). Wiley.
12. Pais, M. and Rao, P. 2021. An up-to-date review on industrially significant inhibitors for corrosion control of zinc. Journal of Bio-and Tribo-Corrosion, 7: 117.
13. Pattanayak, P., Behera, P., Das, D. and Panda, S.K. 2010. *Ocimum sanctum* Linn. A reservoir plant for therapeutic applications: An overview. Pharmacognosy Reviews, 4(7): 95-105.
14. Popova, A., Sokolova, E., Raicheva, S. and Christov, M. 2003. AC and DC study of the temperature effect on mild steel corrosion in acid media in the presence of benzimidazole derivatives. Corrosion Science, 45(1): 33-58.
15. Prakash, P. and Gupta, N. 2005. Therapeutic uses of *Ocimum sanctum* Linn (Tulsi) with a note on eugenol and its pharmacological actions: A short review. Indian Journal of Physiology and Pharmacology, 49(2): 125-131.
16. Revie, R.W. and Uhlig, H.H. 2008. Corrosion and corrosion control (4th ed.). Wiley.
17. Silverstein, R.M., Webster, F.X. and Kiemle, D. 2014. Spectrometric identification of organic compounds (8th ed.). Wiley.
18. Vashi, R.T. and Zele, S.A. 2020. Green corrosion inhibitors for zinc—An overview. International Journal of Advances in Engineering and Management, 2(12): 130–142.
19. Wang, C., Sun, S., Ling, Y., Tan, H. and He, C. 2024. The corrosion resistance of tartaric-sulfuric acid anodic films on the 2024 Al alloy sealed using different methods. Coatings, 14(6): 733.
20. Zhang, R., Sur, D., Li, K., Witt, J., Black, R., Whittingham, A., Scully, J.R. and Hattrick-Simpers, J. 2024. Bayesian assessment of commonly used equivalent circuit models for corrosion analysis in electrochemical impedance spectroscopy. npj Materials Degradation, 8: 120.

Citation: Kwanchi, I.D., Barminas, J.T., Bassi, K.A. and Rapheal, A. 2026. Electrochemical and Surface Characterization of Zinc Corrosion Inhibition by *Ocimum sanctum* Leaf Extract in Hydrochloric Acid. International Journal of Recent Innovations in Academic Research, 10(3): 153-162.